Quantum and transport mobilities of a Na_3Bi-based three-dimensional Dirac system

H. F. Yuan,[1,2] W. Xu,[1,3,*] X. N. Zhao,[1,2] D. Song,[1,2] G. R. Zhang,[1] Y. M. Xiao,[3] L. Ding,[3] and F. M. Peeters[3,4]

[1]*Key Laboratory of Materials Physics, Institute of Solid State Physics, Chinese Academy of Sciences, Hefei 230031, China*

[2]*Science Island Branch of Graduate School, University of Science and Technology of China, Hefei 230026, China*

[3]*Department of Physics and Astronomy and Yunnan Key Laboratory for Quantum Information, Yunnan University, Kunming 650091, China*

[4]*Department of Physics, University of Antwerp, Groenenborgerlaan 171, B-2020 Antwerpen, Belgium*

(Received 29 January 2019; revised manuscript received 20 May 2019; published 17 June 2019)

The electronic and transport properties of a three-dimensional (3D) Dirac system are investigated theoretically, which is motivated by recent experimental measurements on quantum and transport mobilities in the 3D Dirac semimetal Na_3Bi by J. Xiong *et al.* [Science **350**, 413 (2015); Europhys. Lett. **114**, 27002 (2016)]. The electron Hamiltonian is taken from a simplified $\mathbf{k}\cdot\mathbf{p}$ approach. From the obtained electronic band structure and the Fermi energy, we explain why the anomalous effect induced by the chiral anomaly and the Berry curvature in the energy band can be observed experimentally in magnetotransport coefficients in both low- and high-density samples. Moreover, the quantum and transport mobilities are calculated on the basis of the momentum-balance equation derived from a semiclassical Boltzmann equation with the electron-impurity interaction. The quantum and transport mobilities obtained from this study agree both qualitatively and quantitatively with those measured experimentally. We also examine the electron mobilities along different crystal directions in Na_3Bi and find them largely anisotropic. The theoretical findings from this work can be helpful in gaining an in-depth understanding of the experimental results and of the basic electronic and transport properties of newly developed 3D Dirac systems.

DOI: 10.1103/PhysRevB.99.235303

I. INTRODUCTION

Since the discovery of graphene in 2004 [1], the investigation of Dirac electronic systems has been a fast-growing field of research in condensed matter physics, materials science, electronics, and optoelectronics [2]. Graphene is an ideal two-dimensional (2D) Dirac electronic material that is gapless, massless, and with a linear energy dispersion for electrons in the relatively low-energy regime. As a result, graphene exhibits many unique and interesting physical properties [3] that can be utilized for the realization of advanced electronic and optoelectronic devices [4,5]. In recent years, some unique topological materials that are three-dimensionally akin to 2D graphene have been discovered and realized, and therefore they are called three-dimensional (3D) Dirac systems [6]. For example, it is found that the semimetals Cd_3As_2 [7] and Na_3Bi [8] can be gapless and with roughly linear energy dispersion for conduction and valence bands around the Dirac points. Such 3D Dirac electronic systems have a linear energy spectrum for the bulk states around the Dirac nodes and have a topologically protected surface state. In these materials, if either the crystal inversion symmetry or the time-reversal symmetry is broken, each Dirac node splits into a pair of opposite-chirality Weyl nodes. Unique and interesting physical properties can be explored in these 3D Dirac systems such as the Fermi-arc surface states [9], chiral-pumping effect [10], and magnetoelectric-like effects in plasmonics and optics [11]. Very recently, the 3D quantum Hall effect has been observed in Cd_3As_2-based 3D Dirac semimetal systems [12]. These new and important experimental findings indicate that the field of 3D Dirac systems is very rich in terms of fundamental physics and of potential applications as advanced electronic and optical devices.

At present, the most popularly studied 3D Dirac systems are Cd_3As_2- and Na_3Bi-based semimetal materials. From the viewpoint of physics, the electronic band structures of Cd_3As_2 and Na_3Bi around the Dirac point are basically the same [13,14]. Thus, they exhibit roughly similar physical properties. Hence, we focus our present study mainly on Na_3Bi-based 3D Dirac systems. It is known that Na_3Bi is normally in a hexagonal $P6_3/mmc$ phase (or D^4_{6h}) [13]. There are two nonequivalent Na sites called Na(1) and Na(2). Na(1) and Bi can form layers of simple honeycomb lattice layers that are stacked along the c axis. The Na(2) atoms are inserted between the above-mentioned layers, making connection with the Bi atoms and forming layers of honeycomb lattices. From first-principles calculations [13], we know that Na_3Bi has an inverted band structure and its Fermi surface consists of two isolated Fermi points. Since both time-reversal and inversion symmetries are present, there is fourfold degeneracy at each Fermi point around which the band dispersion can be linearized. High-quality hexagon platelike Na_3Bi crystals with large (001) plane surfaces can be grown from a molten Na flux [15]. Xiong *et al.* carried out high-field magnetotransport measurements on n-type Na_3Bi single crystals with relatively low [16] and high [17] electron densities. They measured the de Haas–van Alphen oscillations and the Shubnikov–de Haas oscillations along with the Hall resistance in different samples with and without postannealing. They found that

*wenxu_issp@aliyun.com

both the conductivity and resistivity tensors exhibit robust anomalies in the presence of high magnetic fields in both low- and high-density cases. They found that the longitudinal resistivity depends roughly linearly on the strength of the magnetic field up to 35 T, while the Hall angle exhibits an unusual profile approaching a step function. It is known that the large negative longitudinal magnetoresistance associated with the chiral anomaly is most pronounced in Na_3Bi crystals when the Fermi level is close to the Dirac nodes. This effect occurs in the low-density case [16]. However, as pointed out by Xiong and co-workers [17], even in samples with relative high electron density or high Fermi level away from the Dirac points, the finite Berry curvature seems to lead to major anomalous features in the elements of the conductivity tensor in Na_3Bi. This has led to a reexamination of the electronic transport properties in Na_3Bi-based Dirac semimetals [17]. Furthermore, from high-field magnetotransport measurements, the effective electron mass, the Fermi velocity, the electron density, and the quantum and transport mobilities for different Na_3Bi samples were obtained experimentally [17]. It was found that similarly to the case of a 2D Dirac system such as graphene, the transport mobility is larger than the quantum mobility in the Na_3Bi semimetal.

Motivated by these interesting and important experimental findings, we present here a detailed theoretical study on electronic and transport properties of the semimetal Na_3Bi. Although some theoretical studies on electronic band structure and related electronic properties of 3D Dirac systems have been published [13], there is a lack of a systematic theoretical investigation of the electronic transport properties of Na_3Bi. In this study, we employ a simple and apt theoretical approach to examine the many-body effects such as the electronic screening length and the electron-impurity interaction. We also calculate the quantum and transport mobilities in Na_3Bi at low temperatures. The prime motivation of the present theoretical study is to gain an in-depth understanding of the experimental results on electronic and transport properties of Na_3Bi-based 3D Dirac systems.

This paper is organized as follows. The theoretical approaches to calculate the electronic band structure, the Fermi level, the electronic screening length, and the quantum and transport mobilities in the Na_3Bi semimetal are presented in Sec. II. In Sec. III, we present the numerical results, discuss the electronic and transport properties of Na_3Bi, and compare with those obtained experimentally. The concluding remarks from this study are summarized in Sec. IV.

II. THEORETICAL APPROACH

A. Simplified electron Hamiltonian

In 2012 Wang and co-workers [13] constructed a Hamiltonian to describe the carriers in the semimetal Na_3Bi by using a $\mathbf{k}\cdot\mathbf{p}$ formula, which reads

$$H = \epsilon_{\mathbf{K}} \times I + \begin{bmatrix} M_{\mathbf{K}} & Ak_+ & 0 & B^*_{\mathbf{K}} \\ Ak_- & M_{\mathbf{K}} & B^*_{\mathbf{K}} & 0 \\ 0 & B_{\mathbf{K}} & M_{\mathbf{K}} & -Ak_- \\ B_{\mathbf{K}} & 0 & -Ak_+ & -M_{\mathbf{K}} \end{bmatrix}, \quad (1)$$

where $\mathbf{K} = (\mathbf{k}, k_z) = (k_x, k_y, k_z)$ is the wave vector or momentum operator, I is a 4×4 unitary matrix, $k_\pm = k_x \pm ik_y$, $\epsilon_{\mathbf{K}} = C_0 + C_1k_z^2 + C_2k^2$, $M_{\mathbf{K}} = M_0 - M_1k_z^2 - M_2k^2$, and C_0, C_1, C_2, M_0, M_1, M_2, and A are band parameters [13]. In this Hamiltonian, the stacking direction of the honeycomb lattice layers formed by Na(1) and Bi is taken as the z direction. It should be noted that $B_{\mathbf{K}} = B_3k_zk_+^2$ is a high-order term in the Hamiltonian, which contributes significantly only at relatively large electron momentum. The corresponding Schrödinger equation can be solved analytically. The eigenvalue corresponding to this Hamiltonian is given as $E_\pm(\mathbf{K}) = \epsilon_{\mathbf{K}} \pm (M_{\mathbf{K}}^2 + A^2k^2 + |B_{\mathbf{K}}|^2)^{1/2}$ with the upper (lower) case referring to the conduction (valence) band. This result suggests that there are two Dirac points, determined by $E_+(\mathbf{K}) - E_-(\mathbf{K}) = 0$, in Na_3Bi that are found when taking $k = 0$ and $k_z = \pm k_c = \pm\sqrt{M_0/M_1}$.

It is well known that the $\mathbf{k}\cdot\mathbf{p}$ model is valid for the calculation of the electronic states near the bottom of the conduction band and the top of the valence band [18,19]. Under the action of a relatively weak dc driving electric field, the electronic transport occurs mainly around the Fermi energy, which is normally in the low-energy and small-momentum regime. In such a case, the high-order contribution $B_{\mathbf{K}} \sim K^3 \ll 1$ in Eq. (1) can be neglected. Thus, the 4×4 matrix given by Eq. (1) is decoupled and the electron Hamiltonian is reduced to become a 2×2 matrix, which reads

$$H = \begin{bmatrix} \epsilon_{\mathbf{K}} + M_{\mathbf{K}} & Ak_+ \\ Ak_- & \epsilon_{\mathbf{K}} - M_{\mathbf{K}} \end{bmatrix}. \quad (2)$$

By solving the corresponding Schrödinger equation, the analytical expression for the eigenvalue and eigenfunction for a free carrier in Na_3Bi are obtained, respectively, as

$$E_\lambda(\mathbf{K}) = \epsilon_{\mathbf{K}} + \lambda\sqrt{M_K^2 + A^2k^2} \quad (3)$$

and

$$\Psi_{\mathbf{K}\lambda}(\mathbf{R}) = a_1(1, a_2)e^{i\mathbf{K}\cdot\mathbf{R}}. \quad (4)$$

Here, $\mathbf{R} = (x, y, z)$, $a_1 = \xi_{\mathbf{K}}/(\xi_{\mathbf{K}}^2 + A^2k^2)^{1/2}$, $a_2 = Ak_-/\xi_{\mathbf{K}}^2$, $\xi_{\mathbf{K}} = M_{\mathbf{K}} + \lambda\sqrt{M_{\mathbf{K}}^2 + A^2k^2}$, and $\lambda = +1$ ($\lambda = -1$) refers to the conduction (valance) band. Using this simplified Hamiltonian, two Dirac points are formed when $k = 0$ and $k_z = \pm k_c = \pm\sqrt{M_0/M_1}$. We can prove that the neglect of the $B_{\mathbf{K}}$ term in Eq. (1) does not affect the electronic band structure significantly in the momentum and energy regime in which we are interested (see Sec. III). Hence, for the convenience of the analytical and numerical calculations, in this study we take the electron Hamiltonian given by Eq. (2) for further investigation.

B. Electronic density of states and Fermi energy

With the electronic energy spectrum, the Green's function for an electron in a 3D Dirac system can be written as

$$G_\lambda(E) = P\left(\frac{1}{E - E_\lambda(\mathbf{K})}\right) - i\pi\delta[E - E_\lambda(\mathbf{K})],$$

with P being the principal value, E the electron energy, and $E_\lambda(\mathbf{K})$ the electron energy given by Eq. (3). From now on, we consider the case of an n-type semimetal Na_3Bi in which the

conducting carriers are electrons. By definition, the density of states (DOS) for an electron in an electronic system can be obtained from the imaginary part of the Green's function, which gives

$$D_+(E) = -\frac{g_s}{\pi}\sum_{\mathbf{K}} \mathrm{Im}G_+(E) = \frac{1}{\pi^2}\int_0^\infty dk_z \int_0^\infty dk\, k\, \delta[E - E_+(\mathbf{K})], \quad (5)$$

where $g_s = 2$ counts for spin degeneracy.

Using the electronic DOS, we can determine the corresponding Fermi energy by applying the condition of electron number conservation: $N_e = \int_0^\infty dE D_+(E) f(E) = g_s \sum_{\mathbf{K}} f[E_+(\mathbf{K})]$ with N_e being the electron density, $f(x) = [e^{(x-E_F)/k_BT} + 1]^{-1}$ the Fermi-Dirac function, and E_F the chemical potential (or Fermi energy at $T \to 0$). For the case of an n-type Na_3Bi, at a finite-temperature we have

$$N_e = \frac{1}{\pi^2}\int_0^\infty dk_z \int_0^\infty dk\, k\, f(E_+(\mathbf{K})). \quad (6)$$

Thus, the Fermi energy E_F of a semimetal Na_3Bi can be obtained via root finding from Eq. (6) at the given electron density N_e and temperature T.

C. Random phase approximation screening length

Here we look into some of the related many-body properties of a 3D Dirac system. With the electron wave function, we can calculate the electrostatic energy induced by the bare electron-electron (e-e) interaction:

$$V_0(\mathbf{K}, \mathbf{Q}) = V(\mathbf{K} + \mathbf{Q}, \mathbf{K}; \mathbf{K} - \mathbf{Q}, \mathbf{K}), \quad (7)$$

with

$$V(\mathbf{K}_1', \mathbf{K}_1; \mathbf{K}_2', \mathbf{K}_2) = \int d^3\mathbf{R}_1 d^3\mathbf{R}_2 \Psi^*_{\mathbf{K}_1'+}(\mathbf{R}_1)\Psi_{\mathbf{K}_1+}(\mathbf{R}_1) \times \frac{e^2}{\kappa|\mathbf{R}_1 - \mathbf{R}_2|}\Psi^*_{\mathbf{K}_2'+}(\mathbf{R}_2)\Psi_{\mathbf{K}_2+}(\mathbf{R}_2) = F_0(\mathbf{K}, \mathbf{Q})V_Q,$$

where the momentum conservation law for e-e interaction has been applied [20]; namely, $\mathbf{K}_1 = \mathbf{K}_2 = \mathbf{K}$ are momentums entering into the interaction along with $\mathbf{K}_1{}' = \mathbf{K} + \mathbf{Q}$ and $\mathbf{K}_2{}' = \mathbf{K} - \mathbf{Q}$ being the momentums flowing out of the interaction. Here, $\mathbf{Q} = (q_x, q_y, q_z)$ is the change of electron wave vector or momentum during an e-e interaction event, $V_Q = 4\pi e^2/(\kappa Q^2)$ is the Fourier transformation of the Coulomb potential with κ being the static dielectric constant of Na_3Bi, and $F_0(\mathbf{K}, \mathbf{Q}) = \langle \mathbf{K} + \mathbf{Q}|\mathbf{K}\rangle\langle \mathbf{K} - \mathbf{Q}|\mathbf{K}\rangle$ is the form factor for e-e interaction. The strength of the effective e-e interaction can be calculated through $V_{\mathrm{eff}} = \varepsilon^{-1}(\Omega, \mathbf{Q})V_0(\mathbf{K}, \mathbf{Q})$, where $\varepsilon(\Omega, \mathbf{Q})$ is the dynamical dielectric function matrix with Ω being the excitation frequency. Under the random phase approximation (RPA) the dielectric function matrix can be written as

$$\varepsilon(\Omega, \mathbf{Q}) = 1 - \sum_{\mathbf{K}} V_0(\mathbf{K}, \mathbf{Q})\Pi(\Omega; \mathbf{K}, \mathbf{Q}), \quad (8)$$

with

$$\Pi(\Omega; \mathbf{K}, \mathbf{Q}) = g_s \frac{f[E_+(\mathbf{K} + \mathbf{Q})] - f[E_+(\mathbf{K})]}{\hbar\Omega + E_+(\mathbf{K} + \mathbf{Q}) - E_+(\mathbf{K}) + i\delta}$$

being the pair-bubble or density-density correlation function. Here $f(x)$ is the Fermi-Dirac function. In the long-wavelength limit $Q \to 0$, $F_0(\mathbf{K}, \mathbf{Q}) \simeq 1$, and $V_0(\mathbf{K}, \mathbf{Q}) \simeq V_Q$. Thus, for the static case $\Omega = 0$ the sum of the real part of the pair bubble becomes

$$\eta = -\lim_{Q\to 0} g_s \sum_{\mathbf{K}} \mathrm{Re}\,\Pi(0; \mathbf{K}, \mathbf{Q}) = -g_s \sum_{\mathbf{K}} \left.\frac{\partial f(x)}{\partial x}\right|_{x=E_+(\mathbf{K})}. \quad (9)$$

In the low-temperature limit ($T \to 0$), we have $\partial f(x)/\partial x = -\delta(E_F - x)$ and

$$\eta = \frac{1}{\pi^2}\int_0^\infty dk_z \int_0^\infty dk\, k\, \delta[E_F - E_+(\mathbf{K})]. \quad (9a)$$

Thus, the real part of the static dielectric function can be written as $\mathrm{Re}\,\varepsilon(0, \mathbf{Q}) = 1 + K_s^2(\mathbf{Q})/Q^2$ with $K_s^2(\mathbf{Q}) = -(4\pi e^2/\kappa)\sum_{\mathbf{K}} \mathrm{Re}\,\Pi(0; \mathbf{K}, \mathbf{Q})$ being the square of the inverse screening length. In the long-wavelength $Q \to 0$ limit, we have

$$K_s^2(\mathbf{Q}) \to K_s^2 = \frac{4\pi e^2 \eta}{\kappa}. \quad (10)$$

The screening length $1/K_s$ obtained here can be applied for counting, e.g., the screened e-e interaction and the electron-impurity scattering when the effect of e-e interaction is taken into account.

It should be noted that in the present study, we consider an n-type 3D Dirac system. In the presence of relatively weak driving electric field alone, the effect of electric-field-induced carriers can be neglected. Moreover, at low temperatures the effect of thermal excitation of the carriers is very weak. Thus, under these conditions there are almost no holes presented in the electronic system no matter how big the electron density is. Hence, the electron-hole interaction can be neglected in the present study.

D. Electron-impurity scattering

Experimentally, the quantum mobility or lifetime in an electronic system can normally be determined via the amplitudes of the de Haas–van Alphen oscillations or the Shubnikov–de Haas oscillations measured at low temperatures. At relatively low temperatures, the electron-impurity (e-i) scattering is the principal channel for the relaxation of electrons in an electronic system. For the case where the e-i scattering is caused through the Coulomb potential induced by charged impurities that are 3D-like, the e-i interaction Hamiltonian is given as

$$H_{ei} = \frac{e^2}{\kappa}\frac{1}{|\mathbf{R} - \mathbf{R}_a|}, \quad (11)$$

where $\mathbf{R} = (x, y, z)$ is the coordinate of an electron in Na_3Bi and a charged impurity is located at $\mathbf{R}_a = (x_a, y_a, z_a)$. After assuming that the system can be separated into electrons of interest $|\mathbf{K}\rangle$ and impurities $|\mathcal{I}\rangle$, namely $|\mathbf{K}; \mathcal{I}\rangle = |\mathbf{K}\rangle|\mathcal{I}\rangle$, the e-i interaction potential is obtained, in the absence of e-e

screening, as

$$U(Q,\mathbf{R}_a) = \langle \mathbf{K}^{'};\mathcal{I}|H_{ei}|\mathbf{K};\mathcal{I}\rangle = \langle \mathbf{K}^{'}|\mathbf{K}\rangle \frac{4\pi e^2}{\kappa Q^2}\sqrt{N_i}e^{-i\mathbf{Q}\cdot\mathbf{R}_a}\delta_{\mathbf{K}^{'},\mathbf{K}+\mathbf{Q}}, \quad (12)$$

where $\langle\mathcal{I}|\mathcal{I}\rangle = \sqrt{N_i}$ with N_i being the impurity concentration, $\mathbf{Q} = (q_x, q_y, q_z)$ is the change of electron wave vector during an e-i scattering event, and the term $\delta_{\mathbf{K}^{'},\mathbf{K}+\mathbf{Q}}$ is responsible for momentum conservation of the scattering mechanism. Here we have assumed that the impurities are distributed homogeneously in the Na_3Bi crystal. Using Fermi's golden rule, the electronic transition rate for scattering of an electron from a state $|\mathbf{K}\rangle$ to a state $|\mathbf{K}^{'}\rangle$ due to e-i interaction is obtained in the presence of e-e screening as [20]

$$W(\mathbf{K}^{'},\mathbf{K}) = \frac{2\pi}{\hbar}|U_Q|^2\mathcal{F}_{\mathbf{K}^{'},\mathbf{K}}\delta_{\mathbf{K}^{'},\mathbf{K}+\mathbf{Q}}\delta[E_+(\mathbf{K}^{'}) - E_+(\mathbf{K})], \quad (13)$$

where $U_Q = (4\pi e^2/\kappa)(K_s^2+Q^2)^{-1}$, $Q^2 = (k_z^{'}-k_z)^2 + k^2 + k^{'2} - 2kk^{'}\cos\theta$ is induced by momentum conservation for the scattering, θ is the angle between $\mathbf{k}$ and $\mathbf{k}'$ in the xy plane, and

$$\mathcal{F}_{\mathbf{K}^{'},\mathbf{K}} = |\langle \mathbf{K}^{'}|\mathbf{K}\rangle|^2 = \mathcal{Q}_{\mathbf{K}'\mathbf{K}} + \mathcal{P}_{\mathbf{K}'\mathbf{K}}\cos\theta$$

is the form factor for e-i interaction. Furthermore,

$$\mathcal{Q}_{\mathbf{K}'\mathbf{K}} = \frac{\xi_{\mathbf{K}}^2\xi_{\mathbf{K}'}^2 + A^2k^2k'^2}{\left(\xi_{\mathbf{K}}^2 + A^2k^2\right)\left(\xi_{\mathbf{K}'}^2 + A^2k'^2\right)}$$

and

$$\mathcal{P}_{\mathbf{K}'\mathbf{K}} = \frac{2A^2kk'\xi_{\mathbf{K}}\xi_{\mathbf{K}'}}{\left(\xi_{\mathbf{K}}^2 + A^2k^2\right)\left(\xi_{\mathbf{K}'}^2 + A^2k'^2\right)}.$$

E. Quantum and transport mobilities

In this study, we employ the Boltzmann equation (BE) approach to calculate the electronic transport coefficients of the semimetal Na_3Bi. The semiclassic BE for a 3D electron gas can be written as

$$-\frac{e}{\hbar}\mathbf{F}\cdot\nabla_{\mathbf{K}}f(\mathbf{K}) = g_s\sum_{\mathbf{K}'}[T(\mathbf{K}',\mathbf{K}) - T(\mathbf{K},\mathbf{K}')], \quad (14)$$

where $\mathbf{F}$ is a dc electric field acting on the electron, $f(\mathbf{K})$ is the momentum distribution function (MDF) for an electron in state $|\mathbf{K}\rangle$, and $T(\mathbf{K},\mathbf{K}') = f(\mathbf{K})W(\mathbf{K},\mathbf{K}')$ with $W(\mathbf{K},\mathbf{K}')$ being the electronic transition rate. When the driving electric field is applied along the α direction [$\alpha = (x,y,z)$], we have

$$-\frac{e}{\hbar}\mathbf{F}\cdot\nabla_{\mathbf{K}}f(\mathbf{K}) = -\frac{eF_\alpha}{\hbar}\frac{\partial f(\mathbf{K})}{\partial k_\alpha}.$$

For the first moment, the momentum-balance equation can be obtained by multiplying $g_s\sum_{\mathbf{K}}k_\alpha$ on both sides of the BE given by Eq. (14). It should be noted that the main effect of F_α is to cause the drift velocity v_α of the electron along the α direction. As a result, the electron wave vector in the MDF is shifted by [21] $\mathbf{K}\to\mathbf{K}^* = \mathbf{K} - m_\alpha^*\mathbf{v}_\alpha/\hbar$ with m_α^* being the transport effective mass for an electron along the α direction. Thus, the momentum-balance equation becomes

$$\frac{eN_eF_\alpha}{4\hbar} = \sum_{\mathbf{K}',\mathbf{K}}(k_\alpha^{'}-k_\alpha)f(\mathbf{K}^*)W(\mathbf{K},\mathbf{K}'), \quad (15)$$

where the condition of electron number conservation $N_e = g_s\sum_{\mathbf{K}}f(\mathbf{K})$ has been applied. For the case of a weak driving field F_α, the drift velocity of the electron is small so that

$$f(\mathbf{K}^*) \simeq f(\mathbf{K}) - \frac{m_\alpha^*v_\alpha}{\hbar}\frac{\partial f(\mathbf{K})}{\partial k_\alpha}.$$

Due to the symmetry of the electronic energy spectrum in a 3D Dirac system, we have $\sum_{\mathbf{K}',\mathbf{K}}(k_\alpha^{'}-k_\alpha)f(\mathbf{K})W(\mathbf{K},\mathbf{K}') = 0$, and Eq. (15) gives the electron mobility along the α direction: $\mu_\alpha = -v_\alpha/F_\alpha = e\tau_\alpha/m_\alpha^*$, where the momentum relaxation time τ_α is determined by

$$\frac{1}{\tau_\alpha} = \frac{4}{N_e}\sum_{\mathbf{K}',\mathbf{K}}(k_\alpha^{'}-k_\alpha)W(\mathbf{K},\mathbf{K}')\frac{\partial f(\mathbf{K})}{\partial k_\alpha}. \quad (16)$$

After assuming that the electron momentum distribution function can be described by a statistical electron energy distribution (EED) function $f(\mathbf{K}) \simeq f(E_+(\mathbf{K}))$, we have

$$\frac{1}{\tau_\alpha} = \frac{4}{N_e}\sum_{\mathbf{K}',\mathbf{K}}(k_\alpha^{'}-k_\alpha)W(\mathbf{K},\mathbf{K}')\frac{dE_+(\mathbf{K})}{dk_\alpha}\frac{\partial f(x)}{\partial x}\bigg|_{x=E_+(\mathbf{K})}. \quad (17)$$

We take the EED function as the Fermi-Dirac function and in the low-temperature limit ($T\to 0$) we have $\partial f(x)/\partial x = -\delta(x-E_F)$. Thus, for the case of electron-impurity scattering we have

$$\frac{1}{\tau_\alpha} = -\frac{8\pi N_i}{\hbar N_e}\sum_{\mathbf{K}',\mathbf{K}}(k_\alpha^{'}-k_\alpha)\mathcal{F}_{\mathbf{K}'\mathbf{K}}|U_Q|^2\frac{dE_+(\mathbf{K})}{dk_\alpha}\delta_{\mathbf{K}',\mathbf{K}+\mathbf{Q}} \times\delta[E_+(\mathbf{K}')-E_F]\delta[E_+(\mathbf{K})-E_F]$$

$$= -\frac{2N_i}{\pi\hbar N_e}\sum_{\mathbf{k}',\mathbf{k}}(k_\alpha^{'}-k_\alpha)\mathcal{F}_{\mathbf{K}'\mathbf{K}}|U_Q|^2\delta_{\mathbf{K}',\mathbf{K}+\mathbf{Q}} \times\frac{dE(\mathbf{K})}{dk_\alpha}\left|\frac{dE(\mathbf{K}')}{dk_z^{'}}\right|^{-1}_{k_z^{'}=k_0^{'}}\left|\frac{dE(\mathbf{K})}{dk_z}\right|^{-1}_{k_z=k_0},$$

where k_0 is the solution for k_z from $E_F - E_+(\mathbf{K}) = 0$ and $k_0^{'}$ is the solution for $k_z^{'}$ from $E_F - E_+(\mathbf{K}') = 0$. We find $k_0^2 = (s_2 + \sqrt{s_2^2 - s_1s_3})/s_1$ with $s_1 = M_1^2 - C_1^2$, $s_2 = M_1(M_0 - M_2k^2) - C_1(E_F - C_0 - C_2k^2)$, and $s_3 = (M_0 - M_2k^2)^2 - (E_F - C_0 - C_2k^2)^2 + A^2k^2$. Thus, the transport lifetime along the z direction is

$$\frac{1}{\tau_{zt}} = -\frac{N_i}{\pi\hbar N_e}\sum_{\mathbf{k}',\mathbf{k}}\frac{(k_0^{'}-k_0)k_0}{|k_0^{'}k_0|}\frac{\mathcal{F}_{\mathbf{K}'\mathbf{K}}\mathcal{M}_{\mathbf{K}}}{|\mathcal{M}_{\mathbf{K}'}\mathcal{M}_{\mathbf{K}}|}|U_Q|^2\delta_{k_z^{'},k_0^{'}}\delta_{k_z,k_0}, \quad (18)$$

with

$$\mathcal{M}_{\mathbf{K}} = C_1 - \frac{M_1M_{\mathbf{K}}}{\sqrt{M_{\mathbf{K}}^2 + A^2k^2}}.$$

Due to the symmetry of $E_+(\mathbf{K})$ in the xy plane, the electronic lifetimes along the x and y direction should be the same.

The transport lifetime along the x direction is given by

$$\frac{1}{\tau_t} = \frac{N_i}{4\pi^4\hbar N_e}\int_0^\infty dk\int_0^\infty dk'\int_0^\pi d\theta\frac{k^3k'\mathcal{F}_{\mathbf{K}'\mathbf{K}}\mathcal{N}_{\mathbf{K}}|U_Q|^2}{|k_0'k_0||\mathcal{M}_{\mathbf{K}'}\mathcal{M}_{\mathbf{K}}|}\times\left[1-\frac{k'}{k}\cos\theta\right]\delta_{k_z',k_0'}\delta_{k_z,k_0}, \quad (19)$$

where $k_x = k\cos\varphi$, $k_y = k\sin\varphi$, $k_x' = k'\cos(\varphi+\theta)$, and $k_y' = k'\sin(\varphi+\theta)$ have been applied with φ being the angle between $\mathbf{k}$ and the x direction, and

$$\mathcal{N}_{\mathbf{K}} = C_2 - \frac{M_2M_{\mathbf{K}} - A^2}{\sqrt{M_{\mathbf{K}}^2 + A^2k^2}}.$$

Experimentally, the quantum mobility or lifetime is measured in the presence of a quantizing magnetic field, which is obtained though the amplitude of the Shubnikov–de Haas oscillations [17] or the de Haas–van Alphen oscillations [17] with the help of the Dingle plot [22]. Thus, the quantum mobility or lifetime reflects basically the consequences of small-angle scattering within the plane of the cyclotron orbits in an electronic device. In the case in which the magnetic field is applied perpendicular to the honeycomb lattice layer (i.e., the xy plane) of the Na_3Bi crystal, the Landau levels are formed in the xy plane. As a result, the quantum mobility or lifetime can be measured along the x or y direction [17] and reflects the features of small-angle scattering in the xy plane. By considering that the quantum lifetime along the x direction τ_q is induced by small-angle scattering in the xy plane [23], we have the quantum lifetime along the x direction as

$$\frac{1}{\tau_q} = \frac{N_i}{4\pi^4\hbar N_e}\int_0^\infty dk\int_0^\infty dk'\int_0^\pi d\theta\times\frac{k^3k'\mathcal{F}_{\mathbf{K}'\mathbf{K}}\mathcal{N}_{\mathbf{K}}|U_Q|^2}{|k_0'k_0||\mathcal{M}_{\mathbf{K}'}\mathcal{M}_{\mathbf{K}}|}\delta_{k_z',k_0'}\delta_{k_z,k_0}. \quad (20)$$

It should be noted that in sharp contrast to the case of a 2D Dirac system such as graphene in which relatively simple analytical expressions for quantum and transport lifetimes can be derived [20], the quantum and transport lifetimes for a 3D Dirac system are more complicated because of the 3D nature of the electronic system and because of the more complicated electronic energy spectrum.

III. RESULTS AND DISCUSSION

For our numerical calculations in this study, we take the band parameters for the semimetal Na_3Bi as given in Ref. [13]: $C_0 = -0.06382$ eV, $C_1 = 8.7536$ eVÅ^2, $C_2 = -8.4008$ eVÅ^2, $M_0 = -0.08686$ eV, $M_1 = -10.6424$ eVÅ^2, $M_2 = -10.3610$ eVÅ^2, and $A = 2.4598$ eVÅ. These parameters are determined by fitting the energy spectrum of the effective Hamiltonian given by Eq. (1) with those obtained from *ab initio* calculations. It should be noted that in the theoretical model, the energy at the bottom of the conduction band is achieved by taking $k = 0$ and $k_z = \pm k_c$, which is at $E_0 = E_+(0,\pm k_c) = C_0 + C_1M_0/M_1 = 7.6$ meV for Na_3Bi. Because of the linear energy dispersion near the $\pm k_c$ points, we cannot define the band effective mass for an electron in the unusual way $1/m_\alpha^* = \hbar^{-2}[\partial^2E_+(\mathbf{K})/\partial k_\alpha^2]$. In this study, we deal with the case of electronic transport in relatively high density samples in which the Fermi level is well above the Dirac points. As a result, we can take the transport effective mass for an electron in calculating the Fermi energy and the transport coefficients. It has been found experimentally that the transport effective mass for an electron in Na_3Bi is $m_x^* \simeq m_y^* \simeq m_z^* \simeq m^* = 0.11m_e$ (m_e is the rest electron mass), which is determined by the de Haas–van Alphen oscillations in high B-field magnetotransport measurements [17]. The static dielectric constants along the x/y and z axis are found to be, respectively, 5.99 and 5.73 [24]. Because the difference of the dielectric constants along the different directions is relatively small, we take $\kappa = 5.99$ in the calculation. We would like to note that for the calculation of the quantum and transport mobilities along different crystal directions, we only need to take the impurity concentration N_i to be a fitting parameter.

In Fig. 1, we show the conduction band energy given by Eq. (1) as a function of k and k_z for different values of B_3 (left panel). We also show the energy as a function of k_z for $k = 0$ (right panel) in order to see more clearly the effect of the Berry curvature. It should be noted that in the theoretical model, the minimum value of the bottom of the conduction band is achieved by taking $k = 0$ and $k_z = \pm k_c$, which is at $E_0 = 7.6$ meV. Thus, in this study we take $E_0 = 7.6$ meV as a reference for measuring the electron energy. From Fig. 1 we note the following features: (i) Two Dirac points can be found at the bottom of the conduction band when $k_z = \pm k_c$ and $k = 0$. (ii) The energy splitting induced by the presence of the $B_{\mathbf{K}} = B_3k_zk_+^2$ terms in Eq. (1) is rather weak for the case of relatively small k. Even if we take $B_3 = 50$ eVÅ^3 and 100 eVÅ^3, which are rather large values for Na_3Bi, the effect of band splitting is still very small. This is similar to the case of Cd_3As_2-based 3D Dirac systems in which the effect of band splitting is weak [14]. (iii) When $B_3 = 0$, the results shown in Fig. 1 correspond to a simplified electron Hamiltonian given by Eq. (2). This motivates us to employ Eq. (2) as the basis for further calculations in the present study. (iv) Because of the presence of the Berry curvature in a 3D Dirac system, the electronic energy spectrum in the conduction band looks archlike when $k_z = [-k_c, k_c]$. Therefore, in contrast to a conventional 3D electron gas where the minimum of the conduction band is at $k = 0$ and $k_z = 0$, the top or maximum of the archlike electronic energy spectrum for a 3D Dirac system is reached at $k = 0$ and $k_z = 0$, which is $E_B = C_0 + |M_0| \simeq 23$ meV, as shown in the right panel of Fig. 1. (v) The results shown in Fig. 1 imply that the electronic DOS for $E < E_B$ should be much smaller than that for $E > E_B$.

In Fig. 2, we show the Fermi energy E_F as a function of electron density N_e for Na_3Bi-based 3D Dirac systems at different temperatures and for an ideal 3D electron gas (I3DEG) at $T = 0$. Here the Fermi energy for 3D Dirac system is measured from $E_0 = 7.6$ meV. It can be seen that similarly to an I3DEG with a parabolic band structure $E_+(\mathbf{k}) = \hbar^2K^2/2m^*$, the Fermi energy for a 3D Dirac system increases with electron density but decreases with increasing temperature. We find that the Fermi energy depends weakly on temperature when $T < 10$ K. The theoretical results shown in Fig. 1 and Fig. 2 suggest that when E_F is smaller than

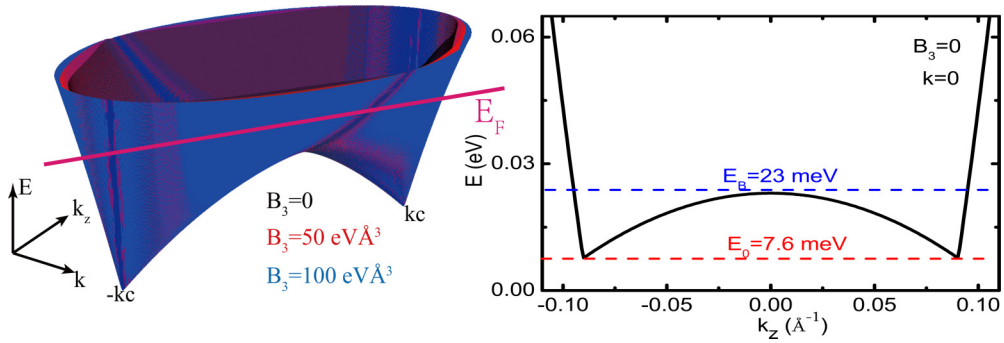

FIG. 1. The energy spectrum of the conduction band as a function of k and k_z for different values of B_3 as indicated (left panel). Here $B_3 \neq 0$ corresponds to the Hamiltonian given by Eq. (1) and $B_3 = 0$ to that given by Eq. (2). The pink line refers to Fermi energy $E_F = 37$ meV calculated by taking $N_e = 4 \times 10^{18}$ cm^{-3} and $T = 4.2$ K. The right panel shows the result for $k = 0$, which also leads to $B_3 = 0$.

$E_0 + E_B = 30.6$ meV, the electrons are mainly located in the energy range with Berry curvature, which corresponds to an electron density $N_e \sim 4 \times 10^{18}$ cm^{-3}. It is known that the presence of Berry curvature in the electronic energy spectrum of the 3D Dirac system is largely responsible for anomalous features in the conductivity tensor elements observed experimentally in Na_3Bi [16,17]. Such an effect can obviously be measured for samples with relatively low electron density so that the Fermi level is below or around the maximum of the Berry curvature as shown in Fig. 1. For samples with low electron densities $N_e \sim 10^{17}$ cm^{-3} in Xiong's experimental work [16], we find theoretically that the Fermi level is in the regime of Berry curvature. For samples with high electron densities $N_e \sim 10^{19}$ cm^{-3} in Xiong's experimental work [17], the theoretical values of the Fermi level are roughly about 50 meV (see Fig. 2), which is above the top of the Berry curvature in the energy spectrum (see Fig. 1). Hence, the difference of the Fermi levels for their low- and high-density samples is only about a factor of 3, instead of 10 times as

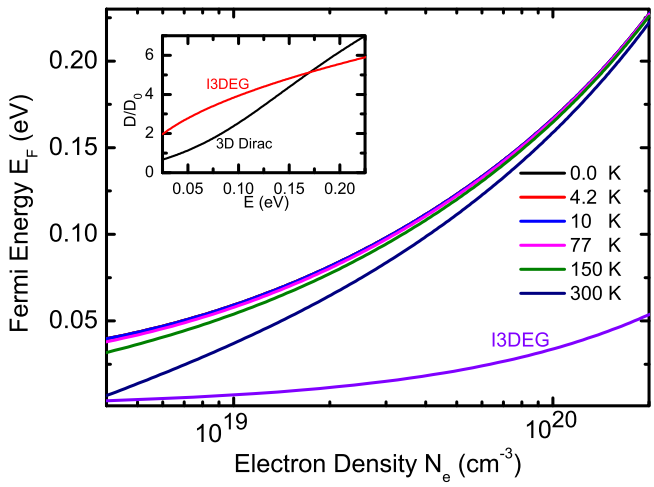

FIG. 2. The Fermi energy E_F in a 3D Dirac system as a function of electron density N_e at different temperatures as indicated. Here we also show the result for an ideal 3D electron gas (I3DEG) at $T = 0$. The results for Na_3Bi 3D Dirac system at $T = 0$ K, 4.2 K, and 10 K coincide roughly. The inset shows the electronic DOS for a 3D Dirac system and for an I3DEG, with $D_0 = C_0^2/A^3$ for 3D Dirac system and $D_0 = m^{*3/2}\sqrt{2|C_0|}/\pi\hbar^3$ for an I3DEG.

was mentioned in Ref. [17]. This becomes the reason why robust anomalies in magnetoconductivities or resistivities can be observed in both their low- and high-density sample cases [16,17]. Moreover, we would like to point out that the energy spectrum for a 3D Dirac system differs very much from that for an I3DEG due to the presence of the Berry curvature. The formula $n_F = g_v k_F^3/3\pi^2$ that Xiong *et al.* used to evaluate the Fermi wave vector k_F or Fermi energy [17] from electron density n_F is derived for an I3DEG. This is why the Fermi energy was overestimated for their high-density samples in their paper. Another point we would like to make is that due to the presence of the Berry curvature in the energy band in 3D Dirac system (see Fig. 1) in the low-energy regime, the effective electronic DOS for a 3D Dirac system is less than that in an I3DEG. Thus, the Fermi energy in a 3D Dirac system is larger than that in an I3DEG at a given electron density as shown in Fig. 2.

Additionally, it should be noted that the robust anomalies in the magnetotransport can also be induced by the presence of a chiral anomaly in 3D Dirac semimetals. It has been demonstrated explicitly [25] that the nonconservation of the number of electrons in the Weyl nodes or Dirac points depends on the chirality of the nodes. Because the electrons with different chiralities move along different directions under the action of perpendicular magnetic field, this feature can lead Landau levels to carry only right or left movers and, consequently, can result in anomalies in magnetoconductivities. Very recently, Thakur *et al.* reported [26] interesting theoretical results for wave-vector- and frequency-dependent longitudinal and transverse current-current response functions for 3D Dirac and Weyl semimetals. They employed these results to examine the impact of chiral anomalies on electronic and plasmonic properties of Weyl semimetals. Basically, the chiral anomaly in a 3D Dirac system or Weyl semimetal can be induced by the joint action of the electric and magnetic fields in the magnetotransport measurement [26]. Because the momentum spacing between two Dirac points is not too large in Na_3Bi (see Fig. 1), the electrons around two Dirac points can interact via, e.g., many-body exchange coupling. Thus, the charge transfer between different Dirac points can occur. Hence, the effective electron densities in different Dirac points or nodes can be different when the Fermi level becomes close to the nodes. More specifically, because the Dirac points are located at $k_z \sim \pm k_c$, the longitudinal conductivities σ_{xx}

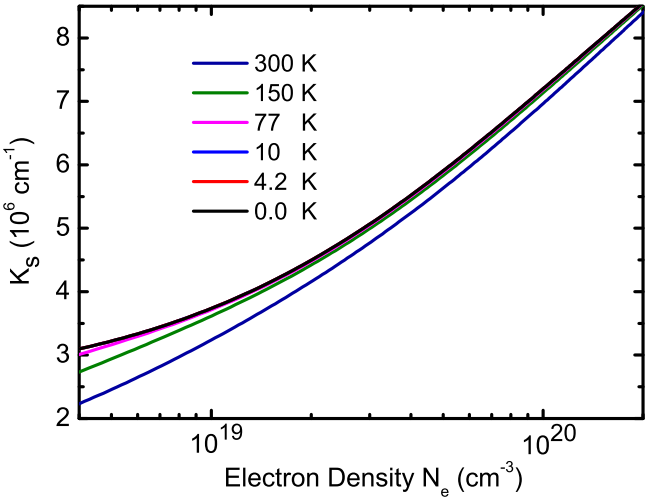

FIG. 3. Inverse screening length K_s as a function of electron density N_e at different temperatures. The results for $T = 0$ K, 4.2 K, and 10 K coincide roughly.

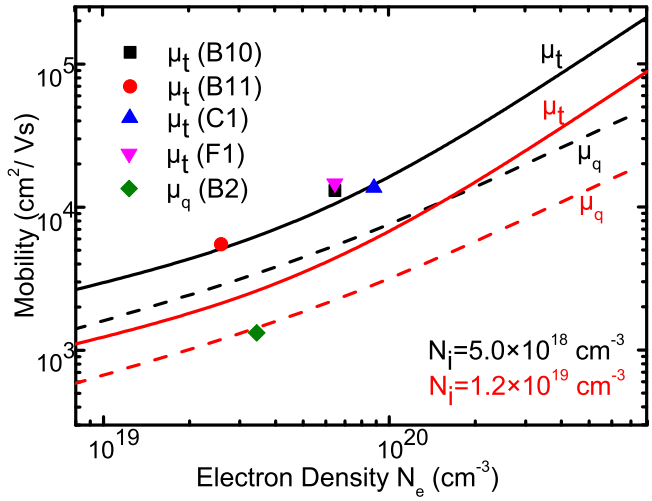

FIG. 4. The quantum μ_q and transport μ_t mobilities as a function of electron density at different impurity concentrations $N_i = 5.0 \times 10^{18}$ cm^{-3} (black curves) and $N_i = 1.2 \times 10^{19}$ cm^{-3} (red curves). The black and red curves are obtained from the present theoretical calculation and the symbols are experimental results [17] with corresponding sample numbers. Note that the experimental result of the quantum lifetime for sample B2 was shown in the caption of Fig. 2 in Ref. [17].

and σ_{yy} can differ significantly from σ_{zz}. Furthermore, the robust anomalies in the Hall resistance [17] R_{xy} are a direct consequence of chiral anomalies in 3D Dirac semimetals. It has been found experimentally that for lower electron density samples (e.g., B6, G1), the chiral-anomaly-affected Hall resistance is more pronounced. This is because the Fermi energy is closer to the Berry curvature regime and to the Dirac points for lower-electron-density samples. Thus, the nonconservation of the number of electrons in the Dirac points with different chiralities can be more significant for a lower-density sample. Consequently, the anomaly in Hall resistance observed experimentally [17] in the Na_3Bi semimetal is the overall contribution from the chiral anomaly, the Berry curvature, and the Fermi energy in the electronic system.

In Fig. 3, we plot the inverse screening length K_s as a function of electron density at different temperatures. The results show that due to the nature of the RPA approach and the nonparabolic electronic energy spectrum, stronger electronic screening is found in a 3D Dirac system with increasing electron density. This is in line with the electronic screening effect found in 2D Dirac systems such as graphene [20] and in monolayer black phosphorus [27]. We find that K_s for Na_3Bi is on the order 10^6 cm^{-1}, which is smaller than that for monolayer black phosphorus and of the same magnitude as graphene. The inverse screening length reflects the strength of the e-e interaction in an electronic system. A larger value of K_s corresponds to a stronger e-e interaction effect. With increasing temperature, because of the thermal broadening of the electronic transitions, the inverse screening length decreases. This behavior is similar to that in I3DEG and in graphene.

In Fig. 4, the quantum and transport mobilities in the xy plane, $\mu_{t/q}$, are shown as a function of electron density for two impurity concentrations $N_i = 5.0 \times 10^{18}$ cm^{-3} (black curve) and $N_i = 1.2 \times 10^{19}$ cm^{-3} (red curves). Here the quantum/transport mobility, $\mu_{q/t}$, is defined as $\mu_{q/t} = e\tau_{q/t}/m^*$. It should be noted that the impurity concentration N_i is the only fitting parameter used in the present calculation. We also show the corresponding experimental results [17] (symbols) for comparison. Here the experimental results for five samples (i.e., B10, B11, C1, F1, and B2) are shown. Experimentally, Na_3Bi samples with different postannealing times were measured at $T = 4$ K, resulting in different values of electron density while having roughly the same impurity concentration. The electron density and mobility of different samples are shown in Table 1 of Ref. [17]. The samples B2, B10, B11, and C1 were measured without postannealing, while sample F1 was postannealed for 2 weeks. It should be mentioned that because of the lattice structure of Na_3Bi and the nature of small-angle scattering measured via high-field magnetotransport experiment, the quantum mobility can only be measured in the xy plane of the semimetal Na_3Bi. We see from Fig. 4 that both μ_q and μ_t increase with increasing electron density N_e. Similarly to other electron gas systems, the electron mobility in Na_3Bi decreases with increasing impurity concentration because a larger N_i leads to a stronger e-i scattering strength. As can be seen from Fig. 4, the theoretical results agree both qualitatively and quantitatively with those obtained experimentally. Due to the nature of small-angle scattering, which can reduce the electronic scattering channels and therefore leads to a shorter lifetime or momentum relaxation time, the quantum mobility is smaller than the transport mobility. This feature is similar to features observed in other electronic systems such as a semiconductor-based 2DEG [23] and graphene [20]. Furthermore, we find that the difference between μ_q and μ_t in the semimetal Na_3Bi increases slightly with electron density and is less than a factor of three even in high-density regimes. It is known that the difference between μ_t and μ_q in semiconductor-based 2DEG systems can be up to 10 times [23]. In a 3D Dirac system, the presence of the electronic scattering channels along the z direction can lead

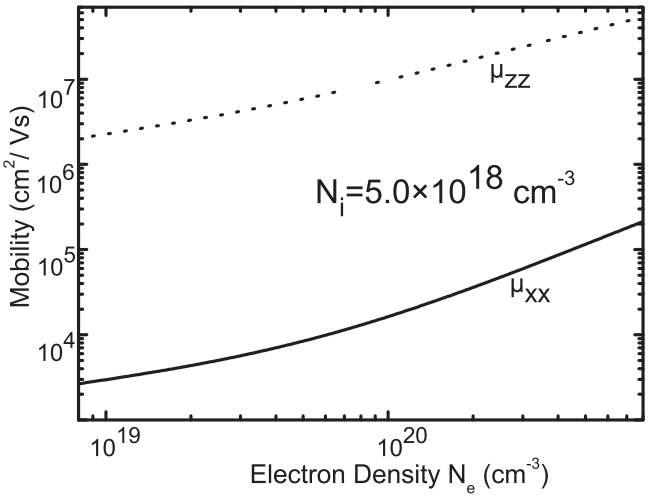

FIG. 5. The transport mobility along the x direction, μ_{xx} (solid curves), and the z direction, μ_{zz} (dashed curves), as a function of electron density N_e for a fixed impurity concentration $N_i = 5.0 \times 10^{18}$ cm^{-3}.

to a reduction of the effective small-angle scattering in the xy plane. This is the main reason why the difference between μ_t and μ_q in Na_3Bi is much smaller than that in semiconductor-based 2DEG systems.

We note that in Fig. 4, two relatively high impurity concentrations are taken to calculate the quantum and transport mobilities and to compare with experimental results for different samples (i.e., B10, B11, C1, F1, and B2) shown in Ref. [17]. The transport mobilities for samples B6, B12, and G1 shown in Table 1 of Ref. [17] are significantly higher than those for B10, B11, C1, F1, and B2. If we take lower impurity concentrations in the calculation, good fittings of the transport mobilities between theoretical and experimental results can be achieved.

In Fig. 5, we show the transport mobility along different directions as a function of electron density. We find that in the Na_3Bi semimetal, the normal mobility μ_{zz} is larger than the in-plane one μ_{xx}. This anisotropic feature is mainly a consequence of the lattice structure of Na_3Bi, which results in different electronic energy dispersions along the xy plane and the z direction. From Fig. 1, we see that the electronic energy spectrum exhibiting Berry curvature occurs in the wave vector region $k_z = [-k_c, k_c]$. The presence of the Berry curvature in the energy band can reduce considerably the electronic DOS along the z direction and, as a result, reduces the electronic scattering channels along the z direction. It should be noted that as shown in Fig. 1, the Berry curvature in the electronic energy spectrum occurs in a relatively low energy regime in the conduction band when $k \sim 0$ and $k_z = [-k_c, k_c]$ in a 3D Dirac system. As a result, the conductivity tensor can be significantly affected by the Berry curvature effect in relatively low electron density samples in which the Fermi level is around the energy regime with the Berry curvature and Dirac points. Thus, one would expect that the difference between μ_{zz} and μ_{xx} can be further enhanced when reducing electron density in a 3D Dirac system. At low temperatures and weak driving electric fields, the electronic transport properties are determined by electronic transition within a relatively low energy range around the Fermi level. For a 3D Dirac system, the presence of the Dirac points and the Berry curvature in the conduction band can reduce the DOS for the low-energy regime. As a result, the electronic transport is accompanied by electronic transition very close to the Fermi level. For high-density samples with electron density $N_e \sim 10^{19}$ cm^{-3}, the Fermi level is still not too far away from the Dirac points and the top or maximum of the Berry curvature in the electronic energy spectrum. Hence, electronic transport in high-density Na_3Bi samples can still feel features of the 3D Dirac system.

IV. CONCLUDING REMARKS

In this work, we have developed a systematic theoretical approach to evaluate the low-temperature electronic and transport properties of the n-type Na_3Bi semimetal. The electronic band structure, the Fermi energy, the electronic screening length induced by electron-electron interaction, the electron-impurity scattering, and the electron quantum and transport mobilities have been examined. The obtained theoretical results have been applied to understanding recent experimental findings on the quantum and transport mobilities of the 3D Dirac semimetal Na_3Bi. The main conclusions from this study are summarized as follows.

The simplified $\mathbf{k} \cdot \mathbf{p}$ Hamiltonian can be reliably employed as a basis for studying the electronic and transport properties of Na_3Bi. From the calculated electronic band structure and the Fermi energy, we have discussed why the anomalous effect induced by chiral anomalies and the Berry curvature in the electronic energy band can be observed experimentally in magnetotransport experiments for both low- and high-density samples. By taking into account electronic screening induced by electron-electron interaction and electron-impurity scattering, we have calculated the quantum and transport mobilities in Na_3Bi as a function of electron density for different impurity concentrations. The quantum and transport mobilities obtained from this study agree both qualitatively and quantitatively with those measured experimentally by Xiong *et al.* [16,17]. The electron mobilities along different crystal directions exhibit large anisotropy. The most significant conclusion we draw from this study is that for high-density Na_3Bi samples with electron density $N_e \sim 10^{19}$ cm^{-3}, the Fermi level is still not too far away from the Dirac points and from the top of the Berry curvature. Therefore, the electronic transport in relatively high density Na_3Bi samples can still exhibit the features of a 3D Dirac electronic system. We hope the results and discussions presented in this work can be helpful for the understanding of some of the basic electronic and transport properties of newly developed 3D Dirac electronic systems.

ACKNOWLEDGMENTS

This work was supported by the National Natural Science Foundation of China (Grants No. 11574319 and No. U1832153), the Center for Science and Technology of Hefei Academy of Science (Grant No. 2016FXZY002), the Department of Science and Technology of Yunnan Province (Grant No. 2016FC001), and Yunnan University (Grant No. 2016MS14).

[1] K. S. Novoselov, A. K. Geim, S. V. Morozov, D. Jiang, Y. Zhang, S. V. Dubonos, I. V. Grigorieva, and A. A. Firsov, Science **306**, 666 (2004).

[2] M. J. Allen, V. C. Tung, and R. B. Kaner, Chem. Rev. **110**, 132 (2009).

[3] K. S. Novoselov, A. K. Geim, S. V. Morozov, D. Jiang, M. I. Katsnelson, I. V. Grigorieva, S. V. Dubonos, and A. A. Firsov, Nature (London) **438**, 197 (2005).

[4] Y. Q. Wu, K. A. Jenkins, A. Valdes-Garcia, D. B. Farmer, Y. Zhu, A. A. Bol, C. Dimitrakopoulos, W. J. Zhu, F. N. Xia, P. Avouris, and Y.-M. Lin, Nano Lett. **12**, 3062 (2012).

[5] Q. L. Bao, H. Zhang, B. Wang, Z. H. Ni, C. H. Y. X. Lim, Y. Wang, D. Y. Tang, and K. P. Loh, Nat. Photonics **5**, 411 (2011).

[6] S. M. Young, S. Zaheer, J. C. Y. Teo, C. L. Kane, E. J. Mele, and A. M. Rappe, Phys. Rev. Lett. **108**, 140405 (2012).

[7] M. Neupane, S. Y. Xu, R. Sankar, N. Alidoust, G. Bian, C. Liu, I. Belopolski, T. R. Chang, H. T. Jeng, H. Lin, A. Bansil, F. C. Chou, and M. Z. Hasan, Nat. Commun. **5**, 3786 (2014).

[8] Z. K. Liu, B. Zhou, Y. Zhang, Z. J. Wang, H. M. Weng, D. Prabhakaran, S.-K. Mo, Z. X. Shen, Z. Fang, X. Dai, Z. Hussain, and Y. L. Chen, Science **343**, 864 (2014).

[9] S. Y. Xu, C. Liu, S. K. Kushwaha, R. Sankar, J. W. Krizan, I. Belopolski, M. Neupane, G. Bian, N. Alidoust, T. R. Chang, H. T. Jeng, C. Y. Huang, W. F. Tsai, H. Lin, P. P. Shibayev, F. C. Chou, R. J. Cava, and M. Z. Hasan, Science **347**, 294 (2015).

[10] S. Ebihara, K. Fukushima, and T. Oka, Phys. Rev. B **93**, 155107 (2016).

[11] P. E. C. Ashby and J. P. Carbotte, Phys. Rev. B **89**, 245121 (2014).

[12] C. Zhang, Y. Zhang, X. Yuan, S. H. Lu, J. L. Zhang, A. Narayan, Y. W. Liu, H. Q. Zhang, Z. L. Ni, R. Liu, E. S. Choi, A. Suslov, S. Sanvito, L. Pi, H.-Z. Lu, A. C. Potter, and F. X. Xiu, Nature (London) **565**, 331 (2019).

[13] Z. J. Wang, Y. Sun, X. Q. Chen, C. Franchini, G. Xu, H. M. Weng, X. Dai, and Z. Fang, Phys. Rev. B **85**, 195320 (2012).

[14] Z. Wang, H. Weng, Q. Wu, X. Dai, and Z. Fang, Phys. Rev. B **88**, 125427 (2013).

[15] S. K. Kushwaha, J. W. Krizan, B. E. Feldman, A. Gyenis, M. T. Randeria, J. Xiong, S. Y. Xu, N. Alidoust, I. Belopolski, T. Liang, M. Z. Hasan, N. P. Ong, A. Yazdani, and R. J. Cava, APL Mater. **3**, 041504 (2015).

[16] J. Xiong, S. K. Kushwaha, T. Liang, J. W. Krizan, M. Hirschberger, W. D. Wang, R. J. Cava, and N. P. Ong, Science **350**, 413 (2015).

[17] J. Xiong, S. Kushwaha, J. Krizan, T. Liang, R. J. Cava, and N. P. Ong, Europhys. Lett. **114**, 27002 (2016).

[18] J. M. Luttinger, Phys. Rev. **102**, 1030 (1956).

[19] E. O. Kane, J. Phys. Chem. Solids **1**, 249 (1957).

[20] H. M. Dong, W. Xu, Z. Zeng, T. C. Lu, and F. M. Peeters, Phys. Rev. B **77**, 235402 (2008).

[21] W. Xu, F. M. Peeters, and J. T. Devreese, Phys. Rev. B **43**, 14134 (1991).

[22] See, e.g., R. Fletcher, J. J. Harris, C. T. Foxon, and R. Stoner, Phys. Rev. B **45**, 6659 (1992).

[23] J. P. Harrang, R. J. Higgins, R. K. Goodall, P. R. Jay, M. Laviron, and P. Delescluse, Phys. Rev. B **32**, 8126 (1985).

[24] M. Dadsetani and A. Ebrahimian, J. Electron. Mater. **45**, 5867 (2016).

[25] H. B. Nielsen, Phys. Lett. B **130**, 389 (1983).

[26] A. Thakur, K. Sadhukhan, and A. Agarwal, Phys. Rev. B **97**, 035403 (2018).

[27] F. W. Han, W. Xu, L. L. Li, C. Zhang, H. M. Dong, and F. M. Peeters, Phys. Rev. B **95**, 115436 (2017).